Pergamon

Int. J. Heat Mass Transfer. Vol. 39, No. 18, pp. 3791–3797, 1996

0017-9310/96 $15.00+0.00

PII: S0017-9310(96)00064-6

Condensation on a spray of water drops: a cell model study—II. Transport quantities

L. J. HUANG, P. S. AYYASWAMY† and SRINIVAS S. SRIPADA

Department of Mechanical Engineering and Applied Mechanics, University of Pennsylvania, Philadelphia, PA 19104-6315, U.S.A.

(*Received* 20 *November* 1995 *and in final form* 8 *February* 1996)

Abstract—The formulation for a unit cylinder cell model that was used to analyze the hydrodynamics and heat transfer associated with steam condensation on a spray of equal sized water droplets was presented in part I of this study. In this part II, we report the results and discussions for the condensation induced interfacial velocities, surface shear stress, Nusselt number and the Sherwood number. The heat transport in both phases and the species transport in the continuous phase have been treated as transient processes. The interactions between neighboring drops have been examined. Numerically obtained transport results have been compared with an experimental study. Results for a representative spray show that the use of correlations developed for an isolated drop to predict condensation spray behavior may be inaccurate, although isolated drop studies continue to merit investigations. Copyright © 1996 Elsevier Science Ltd.

1. INTRODUCTION

Some of the earliest attempts to study condensing sprays include the contributions by Tanaka [1], Tanaka *et al.* [2] and Ohba *et al.* [3]. Photographic techniques were employed by Tanaka *et al.* [2] to experimentally investigate sprays from two different nozzles—the hollow cone type and the full cone cluster type. The coalescence and breakage of spray droplets were not observed in the pictures. The results were documented in terms of the arithmetic mean diameter and the volume-surface (Sauter) mean diameter. The nozzle characteristics, the photographically determined arithmetic means droplet diameter D_a, the volume-surface (Sauter) mean diameter D_{vs}, the Reynolds numbers based on D_a and D_{vs} and the terminal velocities were provided in the study. The terminal velocities were determined at 9 m below the spray nozzle. Based on these experimental observations of the droplet sizes and suitable correlation equations for isolated droplets, Tanaka *et al.* [2] have predicted Nusselt and Sherwood numbers. Significant contributions have been made in experimental studies on various aspects of direct-contact condensation as evident in the report by Cumo [4]. In particular, these include a study by Celata *et al.* [5] in which experimental results for condensation of saturated steam on subcooled water droplets with diameters in the 0.3–2.8 mm range have been provided. The injection velocity has been varied from 0.85 to 9.0 m s^{-1} with pressures up to 0.6 MPa. The droplet Reynolds number was in the range $150 < Re_g < 2000$, and photographic observations have indicated droplet oscillation and nonsphericity in several cases. The following equation for the average nondimensional droplet temperature Θ_m (see Pasamehmetoglu and Nelson [6, 7], and Carra and Morbidelli [8] for details) was stated to fit the experimental data:

$$\Theta_m = 1 - \frac{6}{\pi^2}\sum_{n=1}^{\infty}\frac{1}{n^2}\exp\left(-n^2 C\frac{4\pi^2\alpha_g t}{d_0^2}\right), \quad (1)$$

where, C is an 'empirical convective factor' given by Celata *et al.* [5] as

$$C = 0.153(Pe'_g)^{0.454} \quad \text{and} \quad Pe'_g = \frac{dU_0}{\alpha_g}\frac{\mu_g}{\mu_g+\mu_l} \quad (2)$$

and Θ_m is defined as

$$\Theta_m = \frac{T-T_0}{T_\infty - T_0}. \quad (3)$$

In an excellent experimental study, Mayinger and Chávez [9] have employed pulsed laser holography to measure condensation on a spray of refrigerant R113 ($C_2F_3Cl_3$) droplets introduced into an environment consisting of a pure vapor of the same substance. The holograms with short exposure times ($\sim$30 ns) were stated to be able to resolve particle sizes larger than 10λ, where λ is the wavelength of the laser beam used. The flow corresponded to the regime of intermediate to high droplet Reynolds number ($100 \leqslant Re_g \leqslant 3500$). The vapor pressure was varied over a range of reduced pressure ($0.03 \leqslant p_r = p_v/p_c \leqslant 0.3$). A pressure-swirl nozzle that produces a conical spray with varying mass flow rates was employed. The spray was characterized in terms of the arithmetic mean drop diameter D_a and the arith-

† Author to whom correspondence should be addressed.

NOMENCLATURE

C	drag coefficient
C_D	total drag coefficient
d	droplet diameter
h	heat transfer coefficient
$h1$	cell axial forward half-length
$h2$	cell axial rearward half-length
k	thermal conductivity
Le	Lewis number ($= \alpha/D$)
m	mass fraction
m_1	noncondensable mass fraction
Nu	Nusselt number ($= hd/k$)
p	pressure
Pe	Peclet number ($= Ud/\alpha$ or Ud/D)
r	spherical radial coordinate
R	radius of the drop
R_c	radius of the outer boundary
Re	Reynolds number ($= U_\infty d/\nu$)
Sh	Sherwood number ($= h_M d/\rho D$)
T	temperature
u	velocity component
U_∞	free stream velocity
w_1	dimensionless mass fraction ($= m_1/m_{1,s}$)
$w1$	cell radius nondimensionalized by drop radius
W	condensation parameter ($= 1 - m_{1,\infty}/m_{1,s}$).

Greek symbols

α	thermal diffusivity
θ	polar angle
Θ	nondimensional temperature
λ	wavelength
μ	dynamic viscosity
ν	kinematic viscosity
ρ	density
τ	stress tensor
ψ	stream function.

Subscripts

a	arithmetic mean
c	critical
C	condensation
F	friction
g	gaseous phase
l	liquid phase
L	lead drop
m	mean
P	pressure
r	radial direction
S	spray
vs	volume-surface (Sauter) mean
θ	at angular position
0	at initial time
1	noncondensable
∞	far-stream.

Superscripts

′	modified.

metic mean drop velocity U_a. The effect of condensation on the liquid sheet prior to breakup into droplets was taken into account in the study. Plots to show the influence of the vapor pressure on D_a, U_a breakup length, and on the spray angle have been presented. Results for the mean droplet growth in terms of the relative drop size increment as a function of the droplet size class have also been presented. The heat transfer was calculated assuming that all the droplets in the spray have a diameter equal to the Sauter mean diameter D_{vs} and their surface temperature assumed equal to the saturation temperature. Temperatures were measured along various axial locations using thermocouples. The overall heat transfer coefficient was calculated from a computation of the mass condensed on the swarm of droplets. Results for the heat transfer coefficient and condensation rate are included. An uncertainty analysis has also been presented that estimates the hologram resolution error to be less than 1%, the statistical error to be about 7% and the error in the measurement of the bulk liquid temperature between 5 and 30%. The overall error in heat transfer measurement was stated to be in the range 8–23%.

In parts I and II of this study, we have investigated condensation on a spray of water drops using a cylindrical cell model. The physical description, formulation and the solution procedure for the transport processes along with that for the flow have been presented earlier in part I [10] of this study. Here, we concentrate on the transport results.

2. PHYSICAL QUANTITIES OF THE PROBLEM

In this section, equations for obtaining the interfacial velocities, shear stress, Nusselt number, and Sherwood number are provided.

The dimensionless velocity components are given by

$$u_{g,\theta}|_{r=1} = \frac{1}{\sin\theta}\left.\frac{\partial \psi_g}{\partial r}\right|_{r=1} \tag{4}$$

$$u_{g,r}|_{r=1} = -\frac{1}{\sin\theta}\left.\frac{\partial \psi_g}{\partial \theta}\right|_{r=1}. \tag{5}$$

The shear stress is given by

$$\tau_{r,\theta} = \left[r \frac{\partial}{\partial r}\left(\frac{u_{g,\theta}}{r}\right) + \frac{1}{r}\frac{\partial u_{g,r}}{\partial \theta} \right]_{r=1}. \quad (6)$$

The local heat and mass transport are expressed in terms of the dimensionless local Nusselt and Sherwood numbers, respectively. At any angular location θ on the drop surface, these are defined as follows:

$$Nu(\theta) = \left(\frac{2}{1-T_g} \frac{\partial T_g}{\partial r} \right)\Big|_{r=1} \quad (7)$$

and

$$Sh(\theta) = \left(\frac{2}{1-w_1} \frac{\partial w_1}{\partial r} \right)\Big|_{r=1}. \quad (8)$$

The heat and mass transport averaged over the entire surface of a drop are expressed in terms of the dimensionless average Nusselt and Sherwood numbers, respectively. For the ith drop, these are defined as follows:

$$Nu_i = \int_0^{\pi} \left(\frac{1}{1-T_g} \frac{\partial T_g}{\partial r} \right)\Big|_{r=1} \sin\theta \, d\theta \quad (9)$$

and

$$Sh_i = \int_0^{\pi} \left(\frac{1}{1-w_1} \frac{\partial w_1}{\partial r} \right)\Big|_{r=1} \sin\theta \, d\theta. \quad (10)$$

With a knowledge of the velocity field, temperature and species distributions obtained from a numerical solution of the governing equations, we are able to compute the transport quantities.

3. RESULTS AND DISCUSSION

The transport results are presented for various values of Re_g, and spacings between the droplets with $W = 0.41$. In the following discussion, the cells will be identified by the name of the drop it contains, e.g. cell A, cell B, and so on. For the drops A, B, C and D, the variation in surface shear stress with angular location on the drop surface ($\theta = 0$ corresponds to the front stagnation point) is plotted in Fig. 1 for

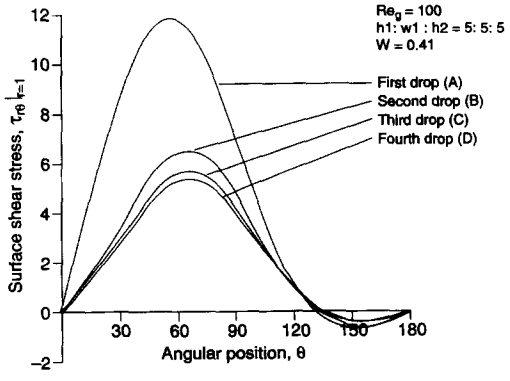

Fig. 1. The variation in surface shear stress $\tau_{r\theta}|_{r=1}$ with angular location for drops A, B, C and D.

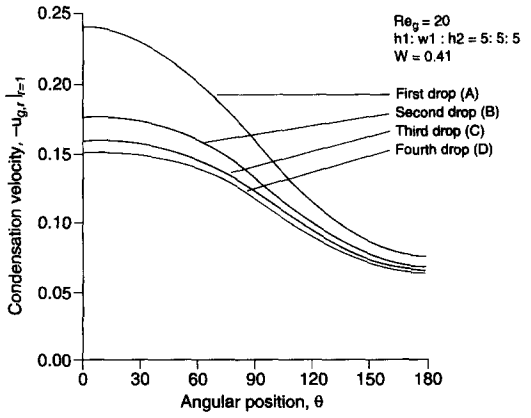

Fig. 2. The variation of surface condensation velocity $-u_{g,r}|_{r=1}$ with angular location for drops A, B, C and D for $Re_g = 20$.

$W = 0.41$, $Re_g = 100$ and $h1 : w1 : h2 = 5 : 5 : 5$. For any given drop, the shear stress increases to a maximum value on the front surface of the drop and then decreases. Beyond the drop equatorial plane, the shear stress becomes negative. For the lead drop, the region of negative shear stress lies in the range $130° < \theta < 180°$. The negative shear stress region exists due to the flow recirculation on the rear of the drop beyond the point of flow separation. The increase in shear stress on the front surface is related to the thinning of the boundary layer (steeper gradients) due to both the vigorous condensation (suction) and the strong translational flow field. At the rear, the flow field and level of condensation are both weaker, the boundary layer is thicker (weaker gradients) and the shear stress is correspondingly lower. For the follower drops B, C and D, the shear stress profiles are similar to that for A, except that the magnitudes are lower in view of the weaker flow fields.

Figures 2 and 3 show the variation of the condensation velocity at the surfaces of the drops, $u_{g,r}|_{r=1}$, with angle θ for $W = 0.41$, $h1 : w1 : h2 = 5 : 5 : 5$ and $Re_g = 20$ and 100, respectively. For the lead drop A,

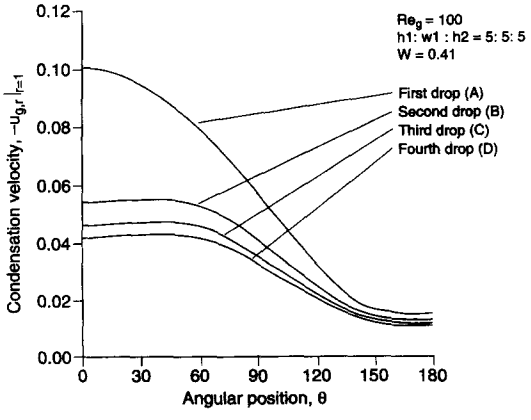

Fig. 3. The variation of surface condensation velocity $-u_{g,r}|_{r=1}$ with angular location for drops A, B, C and D for $Re_g = 100$.

at both the values of Re_g, the concentration gradient is the steepest at the front stagnation point, and the condensation velocity attains its maximum there. At any angular position, the surface condensation velocity is higher for the leader drop. For a given drop, with increasing angle, the velocity decreases up to the separation ring and varies approximately as $\cos\theta$. The effect of translation on condensation is least felt at the separation ring in view of the small local velocity. Most of these features are also present with the second and subsequent follower drops with a major exception. As can be seen in Fig. 3, at the larger value of $Re_g = 100$, the maximum condensation velocity and hence, the steepest concentration gradient do not occur at the front stagnation points of the follower drops. This is ascribable to the effects of wake recirculation at the rear of the leader drop on the flow experienced by the follower drop. These effects are such as to not only reduce the extent of convective mass transfer on the front portion of the follower drop(s), but also to cause the steepest gradient to occur at points away from the front stagnation point.

In Fig. 4 the surface tangential velocity, $u_{g,\theta}|_{r=1}$, is plotted against angular position θ, for drops A, B, C and D, with $W = 0.41$, $Re_g = 100$, and $h1 : w1 : h2 = 5 : 5 : 5$. The tangential velocity varies approximately as $\sin\theta$. We note that the lead drop has a more vigorous internal vortex motion compared with the vortex motion inside drops B, C and D, because of the larger surface shear stress experienced by the lead drop.

The local variation of the Nusselt number $Nu(\theta)$ and Sherwood number $Sh(\theta)$ with angular position θ for a row of drops are shown in Figs. 5 and 6, respectively. The parameter values are $W = 0.41$, $Re_g = 100$, and $h1 : w1 : h2 = 5 : 5 : 5$. Since the Lewis number Le (ratio of thermal and species diffusivities) is of order 1, these two profiles appear to be similar. At the front stagnation point of the lead drop, where the concentration and temperature gradients are the steepest, $Nu(\theta)$ (Fig. 5) and $Sh(\theta)$ (Fig. 6) attain the maximum values. With increasing angle, $Nu(\theta)$ and $Sh(\theta)$

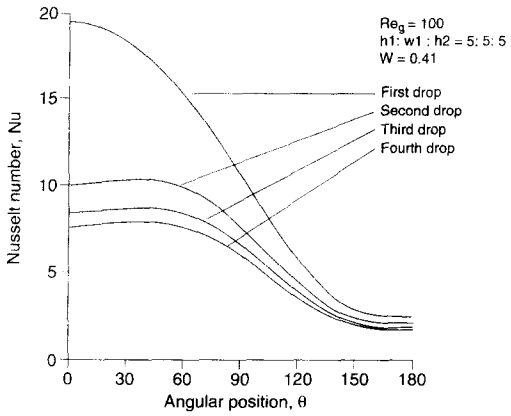

Fig. 5. The variation of local Nusselt number Nu with angular location for drops A, B, C and D.

decrease up to the separation ring and vary approximately as $\cos\theta$. Most of these features are common to the follower drops, except that, as for the case of surface normal velocity, the steepest temperature and concentration gradients do not necessarily occur at the front stagnation points. As a result, the maximum values for $Nu(\theta)$ and $Sh(\theta)$ may not occur at the front stagnation points. The shift in the location of the steepest gradient is primarily ascribable to the wake effects of the leader drops. It must be noted that for a particular W, this shift is seen only for a high enough value of the Reynolds number.

The shear stress associated with a row of the drops is also strongly influenced by the presence of drops on the sides. If the side drops are sufficiently distant from any given drop, for example, $w1 > 10$ for $Re_g = 100$, the effects of the side drops are negligible. The variation in shear stress over the surface of lead drop A, $\tau_{r\theta}|_{r=1}$, with angle θ taking into account the presence of the side drops is plotted in Fig. 7. The parameters are $Re_g = 100$ and $W = 0.41$ for various aspect ratios. On the front portion of drop A, the shear stress is higher with increasing proximity of the side drops. This is as expected due to the increase of friction. The

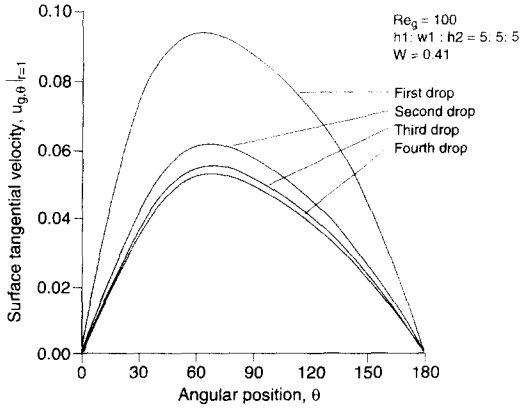

Fig. 4. The variation of surface tangential velocity $u_{g,\theta}|_{r=1}$ with angular location for drops A, B, C and D for $Re_g = 100$.

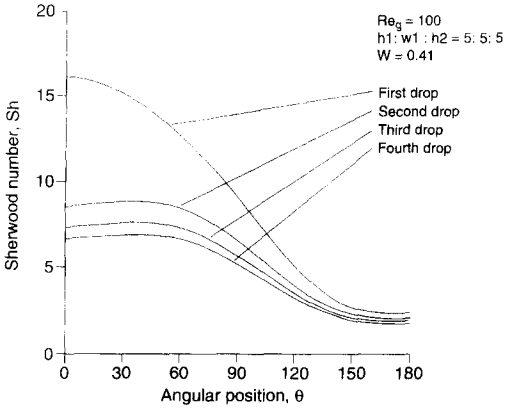

Fig. 6. The variation of local Sherwood number Sh with angular location drops A, B, C and D.

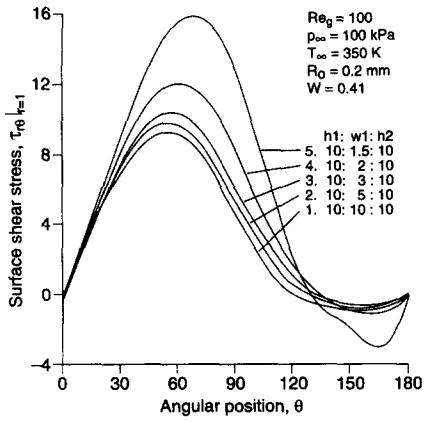

Fig. 7. The variation of surface shear stress $\tau_{r,\theta}|_{r=1}$ for the lead drop with the angular location for various lateral spacings of the side drops.

region of negative shear stress at the rear of drop A is, as before, related to the wake recirculation.

Comparison with experimental results for sprays

It is difficult to compare the numerical results obtained in the present paper with those from equations (1) and (2) in view of the different flow regimes in the cases examined. However, some comparisons with nozzle experimental results are possible. A comparison with the results of Mayinger and Chávez is also not possible due to three reasons namely, (1) the choice of fluid, (2) their consideration only of a pure vapor environment, and (3) the range of reduced pressures considered by them.

As noted earlier, droplet sprays have been experimentally studied using photographic techniques by Tanaka *et al.* [2]. Two different nozzles—NIIKURA 1EX554-L-IC (hollow cone type) and NIIKURA 11/2FG4200K (full cone cluster type)—were used in the experiment. The largest droplet sizes produced were 1.7 mm for NIIKURA 1EX554-L-IC and 1.5 mm for NIIKURA 11/2FG4200K. The initial velocity of spray was 23.5 m s^{-1} (NIIKURA 1EX554-L-IC) and 11 m s^{-1} (NIIKURA 11/2FG4200K), and the initial temperature of the droplets was 40°C. The temperature of the spray environment varied from 60 to 100°C. To document their results, Tanaka *et al.* [2] introduced the arithmetic mean diameter of the spray drop as given by

Table 1. Nozzle characteristics

NIIKURA nozzle	Flow rate ($m^3\ s^{-1}$)	Discharge pressure (MPa)
1EX554-L-IC	9.64×10^{-4}	0.275
11/2FG4200K	2.38×10^{-3}	0.206

$$D_a = \frac{\Sigma_i (n_i D_i)}{\Sigma_i n_i} \tag{11}$$

and the volume-surface (Sauter) mean diameter as given by

$$D_{vs} = \frac{\Sigma_i (n_i D_i^3)}{\Sigma_i (n_i D_i^2)}. \tag{12}$$

The nozzle characteristics are listed in Table 1. The terminal velocities were determined at 9 m below the spray nozzle and have been used in the computation of the Reynolds numbers.

The photographically determined D_a and the Reynolds numbers based on D_a are listed in Table 2(a). Based on these and using a suitable correlation equation for an isolated droplet, Tanaka *et al.* [2] have predicted the Nusselt and Sherwood numbers. These are also listed in Table 2(a). Table 2(a) additionally provides our numerical results for the lead drop in a spectrum of 15 drops distributed among 3 columns and 5 rows. Each droplet in our spray has been assumed to have the same uniform diameter equal to D_a of Tanaka *et al.* [2]. The subscript (LD) denotes that the transport quantity refers to the lead drop.

The photographically determined D_{vs} and the Reynolds numbers based on D_{vs} are listed in Table 2(b). Based on these and using a suitable correlation equations for an isolated droplet, Tanaka *et al.* [2] have predicted Nusselt and Sherwood numbers. These are listed in Table 2(b). Table 2(b) additionally provides our numerical results for the lead drop in a spectrum of 15 drops distributed among 3 columns and 5 rows. Each droplet in our spray has been assumed to have the same uniform diameter equal to D_{vs} of Tanaka *et al.* [2]. The subscript (LD) denotes that the transport quantity refers to the lead drop.

Next, we introduce spray averaged Nusselt and Sherwood numbers through the following definitions:

Table 2a. Experimental results of Tanaka *et al.* [2] and numerical results for the lead drop based on D_a

NIIKURA nozzle	Tanaka *et al.* D_a (mm)	Re_g based on D_a	Nu_{D_a}	Sh_{D_a}	Assumed uniform spray droplet diameter (mm)	Numerical results for the lead drop (present study) Nu_{LD}	Sh_{LD}
1EX554-L-IC	0.48	62	8.0	8.6	0.48	9.1	7.8
11/2FG4200K	0.53	76	8.9	9.2	0.53	9.8	8.4

Table 2b. Experimental results of Tanaka *et al.* [2] and numerical results for the lead drop based on D_{vs}

NIIKURA nozzle	Tanaka *et al.* D_{vs} (mm)	Re_g based on D_{vs}	$Nu_{D_{vs}}$	$Sh_{D_{vs}}$	Assumed uniform spray droplet diameter (mm)	Numerical results for the lead drop (present study) Nu_{LD}	Sh_{LD}
1EX554-L-IC	0.78	164	13.0	12.2	0.78	13.4	11.3
11/2FG4200K	0.70	132	11.7	11.3	0.70	12.1	10.3

$$\overline{Nu}_S = \sum_{i=1}^{n} \frac{Nu_i}{n}, \quad \text{where } n = 15, \tag{13}$$

where Nu_i is the average Nusselt number for the ith droplet in the spray [see equation (9)]. Similar definitions apply for the spray averaged Sherwood number. The subscript S denotes that the transport quantities from our numerical results have been averaged over the entire spectrum of 15 droplets of uniform size. The over bar refers to average quantities based on all the 15 droplets taken together. In Table 3, these average transport quantities are presented with the assumed uniform diameters of 0.48, 0.53, 0.70 and 0.78 mm.

We note from Table 2(a, b) that for the assumed configuration of the spray, the results of Tanaka *et al.* [2] are similar in value to those for the lead drop in our numerical calculations. However, it may be noted from Table 3 that the presence of multiple drops significantly alters the net heat/mass transport, as evidenced by the lower values for the spray averaged Nusselt and Sherwood numbers. This is ascribable both to the weakening of the flow field and wake effects due to the presence of multiple droplets which are not reflected in an isolated droplet study. In the design of spray systems, it is important to take these hydrodynamic and thermal effects into consideration.

4. SIGNIFICANT CONCLUSIONS

The important conclusions that arise from the studies presented in parts I [10] and part II are:

(1) The condensation velocity has an approximate cosine variation with angle in the front portion of the lead drop. The maximum condensation rate, which occurs at the front stagnation point of the lead drop, is approximately twice the average condensation rate on the drop. However, for the follower drops, this relationship does not hold.

(2) The transport to the drop in the rear region is enhanced by recirculation in the wake for translational Reynolds number of $O(100)$. This enhancement increases with Reynolds number and needs to be given due consideration at high levels of drop translation. Boundary layer analysis (see Sundararajan and Ayyaswamy [11]) cannot accurately predict the transport to the entire surface of the drop.

(3) The flow field for the follower drop is significantly influenced by the wake region of the drop ahead. In fact, the steepest gradients of the temperature and concentration do not occur at the front stagnation points of follower drops as a consequence of the wake effects of leader drops.

(4) The dynamics and heat/mass transfer associated with a row of the drops are strongly influenced by the presence of drops on the lateral sides. If the side drops are sufficiently far away from any given drop (more than 10 times the drop radius), their effects are negligible.

(5) The gaseous phase pressure profile at the surface of a typical drop is influenced drastically by the presence of the side drops. For the parameter range investigated, the pressure recovery at the rear of a typical drop becomes smaller as the lateral drops get closer.

(6) On the front portion of a typical drop, the shear stress is higher with increasing proximity of the side drops. The region of negative shear stress at the rear of a typical drop is related to the wake recirculation.

(7) The coefficients for the friction drag C_F, the condensation drag C_C and the pressure drag C_P for a typical drop increase with the proximity of the side drops. The friction drag coefficient C_F increases due to the increased shear stress. The condensation drag coefficient C_C, which arises owing to the momentum of the radial flow, increases due to increased convective velocity. The pressure drag coefficient C_P increases due to the reduced pressure recovery in the rear.

(8) The averaged numerical results for the spray clearly show that the use of single isolated droplet correlations for describing condensation spray behavior could lead to inaccurate designs of heat transfer equipment.

Table 3. Averaged numerical results for the spray.

Assumed uniform spray droplet diameter (mm)	Averaged numerical results for spray (present study) $\overline{Nu}_S$	$\overline{Sh}_S$
0.48	5.6	5.1
0.53	6.4	5.5
0.70	7.6	6.7
0.78	8.4	7.3

Acknowledgements—The numerical calculations were made on the Pittsburgh Supercomputer under NSF grant ECS-

0000000/8515068. The authors are grateful for the Pittsburgh Supercomputer Center services and to NSF.

REFERENCES

1. M. Tanaka, Heat transfer of a spray droplet in a nuclear reactor containment, *Nucl. Technol.* **47,** 268–281 (1980).
2. M. Tanaka, H. Watanabe, K. Hashimoto, Y. Motoki, M. Naritomi, G. Nishio and S. Kitani, Performance of containment sprays for light water reactors and evaluation of the heat transfer, *Nucl. Technol.* **54,** 54–67 (1981).
3. K. Ohba, H. Kitada and A. Nishiguchi, Direct contact condensation on a high speed spray jet of subcooled water. In *Heat Transfer in Nuclear Reactor Safety* (Edited by S. G. Bankoff and N. H. Afgan), pp. 289–300. Hemisphere, Washington, DC (1982).
4. M. Cumo, *Advances in Heat Transfer*, Vol. 5. ENEA Casaccia Heat Transfer Laboratory, Rome (1990).
5. G. P. Celata, M. Cumo, F. D'Annibale and G. E. Farello, Direct contact condensation of steam on droplets, *Int. J. Multiphase Flow* **17,** 191–211 (1991).
6. K. O. Pasamehmetoglu and R. A. Nelson, Direct contact condensation on liquid droplets during rapid depressurization, Part 1 : quasi-steady solution, *ASME Winter Annual Meeting*, Boston, MA (1987).
7. K. O. Pasamehmetoglu and R. A. Nelson, Transient direct contact condensation on liquid droplets, *ASME-ANS-AIChE National Heat Transfer Conference*, Pittsburgh, PA (1987).
8. S. Carra and M. Morbidelli, Transient mass tranfer onto small particles and drops. In *Handbook of Heat and Mass Transfer* (Edited by N.P. Cheremisinoff), Vol. 2. Gulf, Houston, TX (1986).
9. F. Mayinger and A. Chávez, Measurement of direct-contact condensation of pure saturated vapour on an injection spray by applying pulsed laser holography, *Int. J. Heat Mass Transfer* **35,** 691–702 (1992).
10. S. S. Sripada, P. S. Ayyaswamy and L. J. Huang, Condensation on a spray of water drops : a cell model study—I. Flow description, *Int. J. Heat Mass Transfer* **39,** 3781–3790 (1996).
11. T. Sundararajan and P. S. Ayyaswamy, Heat and mass transfer associated with condensation on a moving drop : solutions for intermediate Reynolds numbers by a boundary layer formulation, *J. Heat Transfer* **107,** 409–416 (1985).